Power-Electronics-Based Mission Profile Emulation and Test for Electric Machine Drive System—Concepts, Features, and Challenges

Ke Ma, *Senior Member, IEEE*, Shihao Xia, Yuhao Qi, *Graduate Student Member, IEEE*, Xu Cai, *Senior Member, IEEE*, Yubo Song, *Senior Member, IEEE*, and Frede Blaabjerg, *Fellow, IEEE*

***Abstract*—In the last decade, significant progress has been made in electrification, especially in the applications of electrical vehicles, renewable energies, and industry automations, which imposed much more complicated working conditions to electric machines as well as the drive converters. More advanced features, such as the control strategies, functionality, stability, and reliability of machine drive systems, need to be characterized and validated. Thus, there is an emerging need to accurately recreate the behaviors of electric machine drive systems from more aspects for comprehensive tests. This article aims to foster and investigate the mission profile emulation technologies for the testing of electric machine drive systems. The key factors of the system to be emulated are first clarified, and then different testing concepts are summarized and compared, including dynamometer test, controller hardware-in-the-loop simulation, power hardware-in-the-loop simulation, and power-electronics-based emulation. The features of power-electronics-based emulation, which is considered as a promising trend, will be further discussed with respect to the degrees of coupling with the drive converter, electric machine models, and control structures. Finally, challenges in the field of mission profile emulation for electric machine drive systems are discussed.**

***Index Terms*—Drive converter, drive system characteristics, electric machine emulation, harmonic, testing.**

I. Introduction

ELECTRIC machines, such as permanent magnet synchronous machines (PMSMs), induction machines, and switched reluctance motors, are gaining popularity in industrial production [1], [2], electrified transportation [3]–[6], and renewable energy generation [7]. A typical three-phase electric machine drive system is shown in Fig. 1. The electric machine is fed by a power electronic converter. On the other side, the electric machine is coupled with a mechanical load via a shaft. The electric machine is regulated by the power electronic converter in various ways, such as field-oriented control [8], [9], direct torque control [10], [11], and variable-voltage and variable-frequency [12].

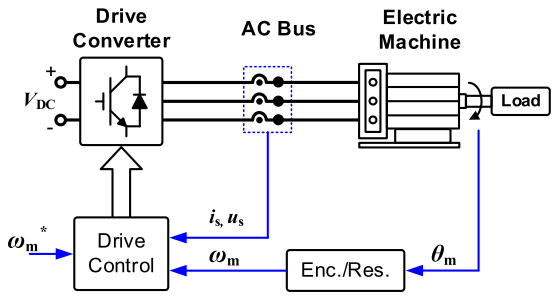

Fig. 1. Typical electric machine drive system. Enc: Encoder. Res: Resolver.

Nowadays, the mission profiles of electric machine drive systems, such as rotational speed changes and load torque, are getting complicated with the advancement of electric machine and converter technologies [13], [14]. Consequently, it is becoming an emerging need to characterize or validate more advanced features of the machine drive system, such as the control strategies, functionality, stability, and reliability [15].

A significant amount of efforts has been made on the testing methods of electric machine drive systems [16]–[25]. A typical approach involves a mechanical load emulator, which is composed of an extra motor and its drive system to establish the required mechanical loads for the electric machine under test [16]–[18]. This typical method is known as dynamometer (Dyno) test, which can be traced back to the 1900s [26]. The Dyno test system can provide a complete drive train and steady-state operating conditions both for the electric machine and for the drive converter. However, the mechanical load emulator is bulky and expensive. Some complicated dynamical behaviors, which are more often seen in real-field applications, are difficult to be generated because of the mismatched inertia and restrained control bandwidth of the mechanical loading system.

Due to these defects, virtualizing tests have become popular solutions to reduce the testing cost and enhance the testing

Manuscript received July 23, 2021; revised January 12, 2022; accepted January 25, 2022. Date of publication February 10, 2022; date of current version March 24, 2022. This work was supported by the National Nature Science Foundation of China under Project 51777123. Recommended for publication by Associate Editor M. Liserre. *(Corresponding author: Ke Ma.)*

Ke Ma, Shihao Xia, Yuhao Qi, and Xu Cai are with the Key Laboratory of Control of Power Transmission and Conversion, Ministry of Education, Shanghai Jiao Tong University, Shanghai 200240, China, and also with the Department of Electrical Engineering, Shanghai Jiao Tong University, Shanghai 200240, China (e-mail: kema@sjtu.edu.cn; xia0112@sjtu.edu.cn; qiyuhao0@sjtu.edu.cn; xucai@sjtu.edu.cn).

Yubo Song and Frede Blaabjerg are with the Department of Energy Technology, Aalborg University, 9220 Aalborg, Denmark (e-mail: yuboso@et.aau.dk; fbl@et.aau.dk).

Color versions of one or more figures in this article are available at https://doi.org/10.1109/TPEL.2022.3149996.

Digital Object Identifier 10.1109/TPEL.2022.3149996

bandwidth. These testing approaches are known as hardware-in-the-loop simulations (HILS), which can be traced back to the 1980s [27]. In a typical HILS, the physical elements, which are not focused as testing targets, are programmed as network models to be real-time calculated by digital processors or simulators. Thus, the prototyping efforts can be efficiently simplified [20]–[23].

The HILS can be further divided into controller hardware-in-the-loop simulations (CHILS) and power hardware-in-the-loop simulations (PHILS) depending on whether the power stage is included or not. For CHILS, the mechanical loads, electric machines, and drive converters are normally programmed as software models to be simulated. The signals are interconnected with the physical controller of the machine drive system. This method is very suitable for the validation of controller and algorithms, but the characteristics related to the power stage cannot be reflected. Different from CHILS, the PHILS includes a power stage with more realistic factors. The mechanical loads and electric machines are programmed as software models. The electrical signals generated by the real-time simulator are recreated as actual power by using a power amplifier to interact with the drive converter. This method is very suitable for the validation of converter design. However, the stability issues of the testing system and high cost for the real-time simulator and power amplifier may prevent PHILS from being widely used [24].

Recently, another group of testing methods named power-electronics-based emulation (PEBE), which were originally known as virtual machines [25], is becoming popular [28]. In this approach, only the terminal characteristics of the voltage and current seen by the drive converter under test (CUT) are focused. An emulating converter is flexibly controlled, and it can recreate the terminal characteristics of electric machine with corresponding behaviors of mechanical loads. Different from PHILS, the PEBE gets rid of the expensive real-time simulator. The models of electric machines and mechanical loads are implemented in the digital controller of the emulating converter.

The above-mentioned testing methods have quite different characteristics as well as suitable testing scenarios. However, the benchmark of different approaches and enabling technologies in this field, are still unclear.

This article aims to give a comprehensive review on the mission profile emulation technologies for electric machine drive systems. The key factors of machine drive systems to be emulated are first clarified, and then different testing concepts are summarized and compared. The features of PEBE, which is considered as a promising trend, are discussed, as well as challenges in the field of mission profile emulation for electric machine drive systems.

The rest of this article is organized as follows. Section II classifies the factors of the electric machine drive systems to be emulated. Different concepts for the electric machine emulation are summarized and compared in Section III, including Concept I: Dyno test, Concept II: CHILS, Concept III: PHILS, and Concept IV: PEBE. Section IV focuses on the features of the PEBE with various configurations. Challenges and existing solutions for PEBE are presented in Section V. Finally, Section VI concludes this article.

II. Typical Factors of Mission Profiles to be Emulated in Electric Machine Drive System

Under different mission profiles, the electric machine will withstand different stresses, which thereby affects the lifetime of the electric machine drive system [29] as it is shown in Fig. 2. These typical factors of mission profiles to be emulated will be discussed as follows.

A. Mechanical Behaviors

Mechanical behaviors include the inertia and vibrations [30]–[33]. The inertia prevents the rotational speed from changing rapidly, and vibrations will cause oscillations in the torque. Basically, mechanical behaviors are much slower than electrical ones due to the mechanical inertia, which may be variable because of the various working conditions. The control performance of the complete drive system is mostly determined by the mechanical behaviors [34], and the control quality can be diminished by them [35], [36]. Thus, it is important to model these mechanical behaviors and accurately reflect the relationship between mechanical and electrical characteristics.

B. Control Strategies and Transients

Control strategies and transients are closely related to the fundamental components of the voltage/current. Basically, the electric machine is regulated by controlling the torque and the rotational speed through the current [8]–[12]. During the regulation, the amplitude and frequency of the fundamental component change with the torque and the speed of revolution. The fundamental component accounts for the most of the voltage/current, and has great impacts on the durability of power electronic converters. Besides, transients will be induced due to changes of mission profiles [37], which challenge the stability and performance of the drive system. In short, the fundamental frequency (f_1) is variable, ranging from tens of Hertz to a few kilo Hertz, and the transients will induce high-frequency oscillations. Thus, high-bandwidth emulation is required. Otherwise, the waveforms will be distorted, leading to unreliable testing results.

C. Electromagnetic Properties

Apart from the fundamental component, harmonics will be excited due to the nonideal characteristics of the electric machine, such as air-gap magnetic field distortion and uneven distribution of magnetic resistance. These undesired characteristics will cause torque ripple and flux distortion, which will have impacts on the stability and performance of the drive system. Together with the fundamental component, these harmonics have impacts on the thermal behaviors of the drive system, which are related to the reliability of the power electronic converters. Typically, harmonics related to nonideal factors are of $6k\pm1$ (k is a positive integer) times of f_1 harmonics in static three phase coordinate [38], [39]. Among them, the 5th and 7th harmonics are dominant [38], which require high-bandwidth and corresponding control algorithms in the emulation system.

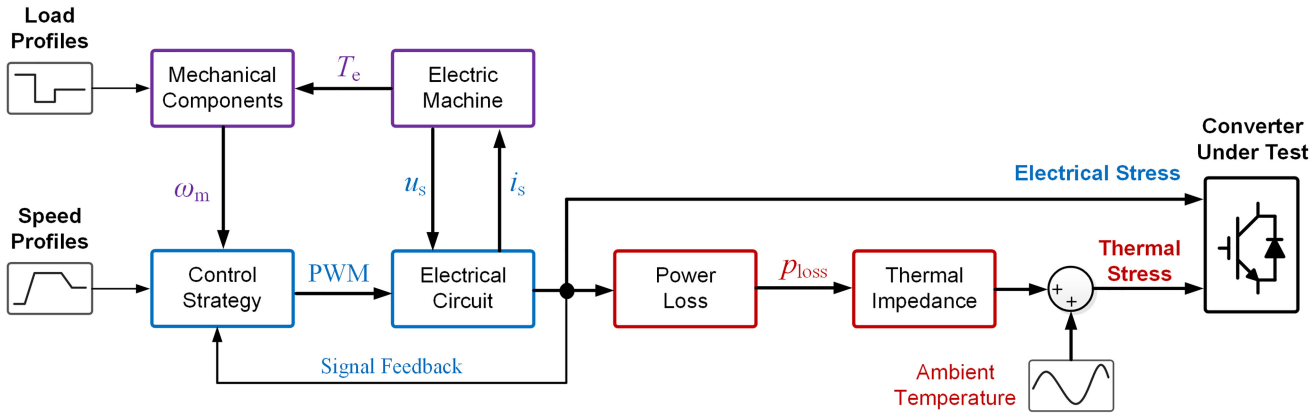

Fig. 2. Stresses imposed to the drive converter under different mission profiles.

D. Abnormal Conditions

Abnormal conditions will appear in voltage and current when faults occur. Typically, the major faults of electric machines can be classified as electrical faults [40], [41] and mechanical faults [33]. Both types of faults will induce irregular voltages and currents [42]. When faults occur, the electric machine will be subjected to transients and harmonics, and so will the drive system. Typically, low-order harmonics of voltage/current are the dominant [40]. These harmonics under faults will have a high amplitude, and will pose great challenges to the reliability of power electronic converters and the performance of drive systems. They may threaten the safety of operators. To reproduce these abnormal behaviors under safe conditions, the reliability and tolerance of the test bench are of vital significance.

E. Environmental Conditions

With more and more electric machines being applied, especially in electric vehicles and aerospace, the working conditions are getting complicated. The environmental factors affecting the reliability and performance of drive systems are mainly temperature and humidity [13], [14]. In the past, they changed with the climate, so the dynamics of their effects were very slow. Nowadays, the bandwidths of temperature and humidity have greatly increased due to the applications in high-speed rail and aerospace, which have a more significant impact. Thus, it is significant to create these multifield coupling environmental conditions when testing the reliability of the electric machine drive system.

III. Concepts of Mission Profile Emulation for Electric Machine Drive System

As it is shown in Fig. 1, a typical electric machine drive system includes drive control, drive converter, electric machine, mechanical load, and power supply. The emulation methods are classified into four concepts.

Concept I is known as the Dyno test and it is shown in Fig. 3(a). In this concept, an extra electric machine, as well as its drive system is used to emulate the characteristics of different loads. Thus, the electric machine drive system can be tested under different load conditions [16]–[18], [43]. In this case, the load machine is coupled to the electric machine under test via a shaft coupler. The desired load torque is achieved by controlling the torque and speed of the load machine.

Concept II is known as CHILS shown in Fig. 3(b). The drive control algorithm is programmed on the drive controller, while other parts are programmed as network models on a real-time simulator. The controller under test and the real-time simulator are connected via signal interfaces, such as analog-to-digital converters (ADC) and digital-to-analog converters (DAC). Because of the flexible model implemented on the real-time simulator, various mission profiles can be recreated in this concept. However, complicated nonideal factors related to power stage are not included in this concept.

Concept III is known as PHILS shown in Fig. 3(c). In PHILS, a power amplifier is connected to the drive converter, whose behaviors are sampled by current/voltage sensors and fed back to the real-time simulator. Then, voltage/current references are generated by the real-time simulator, and transmitted to the controller of the power amplifier. The types of reference signals generated by the real-time simulator and the types of signals sampled by sensors are determined by the interface algorithm. For the voltage-type algorithm, the real-time simulators generate voltage-type references for power amplifier, and current sensors are used to capture current signals. While for the current-type algorithm, the real-time simulators generate current-type references, and voltage sensors are needed.

The electric machine emulation based on Concept IV is named as PEBE. As it is shown in Fig. 3(d), a power electronic converter is flexibly controlled to emulate the behaviors of the desired source or load. Thus, the mechanical parts are substituted by the emulating converter and its control system. Different from PHILS, the model of target electric machine is implemented on the digital controller of the emulating converter, thus avoiding some extra delays in the signal transmissions. The terminal electric characteristics faced by the drive system are the main focus in this concept. These terminal characteristics are recreated by the emulating converter with corresponding control algorithms implemented in the digital controller of the emulating converter.

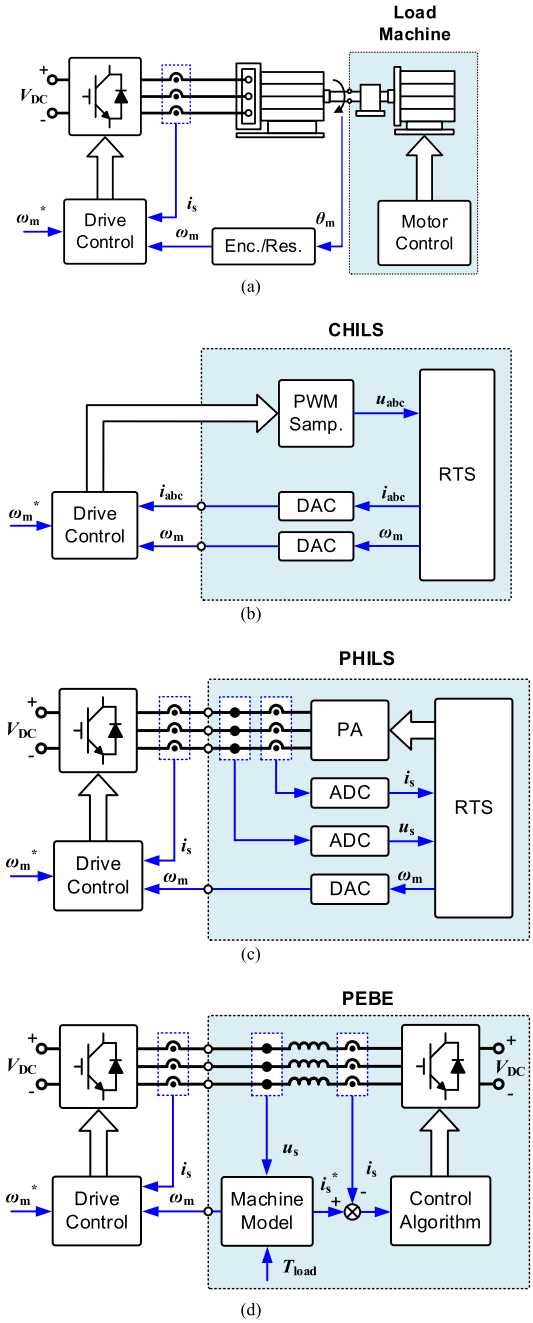

Fig. 3. Four different concepts for testing of electric machine drive systems. (a) Concept I: Dyno test. (b) Concept II: CHILS. (c) Concept III: PHILS. (d) Concept IV: PEBE. RTS: real-time simulator. Gen.: Generation. Samp.: Sampling. DAC: digital-to-analog converters. ADC: analog-to-digital converters. PA: power amplifier.

The major differences among the four concepts are located in the bandwidth of reflected characteristics, stability, power level, testing efficiency, cost, and suitable testing scenarios.

A. Bandwidth of Reflected Characteristics

The bandwidth of reflected characteristics in Concept I is relatively low because of the mechanical inertia. In this concept, the load machine is usually an induction motor, and the inertia is greater than 10^{-4} kg·m^2 [34]–[36], [44] depending on the power level. So, Concept I is unable to present the characteristics of fast dynamics, such as transients and abnormal conditions.

The bandwidth of the reflected characteristics in Concept II is restrained by the time step of real-time simulators and the time step of signal interface modules. The time step of real-time simulators is usually around dozens of μs [45] or a dozen of ns [46], which is similar for signal interface modules. To achieve higher bandwidth of CHILS, signal interface modules with shorter time step are usually adopted. The time step of real-time simulators is normally set to be small. Meanwhile, the model of the system is programmed as network models using parallel processors to achieve shorter time step [23]. In this concept, characteristics related to the electric machine, control strategies and abnormal conditions can be emulated on the real-time simulator.

In Concept III, the bandwidth of the reflected electric machine characteristics is mainly limited by the bandwidth of the power amplifier. This is because the control period of power amplifiers is much larger than the time step of real-time simulators. For PHILS, there are mainly two types of power amplifiers reported in the electric machine emulation: the linear type power amplifier (LPA) and the switched mode power amplifier (SMPA). LPAs work in amplified mode, and can amplify the input signals with a little distortion. The bandwidth of LPAs can reach up to 50 kHz [47]. SMPAs work in switched mode. The widely used two-level converter is commonly adopted due to space and cost. The bandwidth of this topology is usually between hundreds of Hertz and several kilo Hertz [48]–[52]. For Concept III, the characteristics related to the electric machine, control strategies and abnormal conditions can be emulated.

The bandwidth of reflected characteristics in Concept IV is determined by the control period of the emulating converter. Thus, the bandwidth of Concept IV is close to that of PHILS adopting SMPAs.

B. Stability and Robustness to Faulted CUT

The stability and robustness of the electric machine emulation is vital, especially when high power stage or even mechanical structures are involved.

Concept I is actually an electric machine loaded with a programmable load. Thus, the stability of this system depends on the stability of the components and controls for both the electric machine under test and the load machine. The load machine should be coupled to the electric machine tightly to avoid load dump. The inertia of the load machine should match with the inertia of the electric machine to avoid the possible mechanical instability in dynamics [34]. Besides, protections must be triggered in case of faulted converter under test or erroneous control signals. Otherwise, the electric machine may be damaged, and the safety of the operators may be threatened.

The additional delays introduced in Concept II may cause different stability issues [53]. There are three possible delays in Concept II, i.e., the input transmission delay between real-time simulators and drive controllers, the computational delay of the real-time simulators, and the output transmission delay between drive controllers and real-time simulators. The computational

delay is the inherent latency of real-time simulators, and the input transmission delay and output transmission delay may cause oscillations in the waveforms [53]. As to the failures of converter under test, the simulator is hard to be damaged by faulted signals, and can continue to operate as long as the failure model is available.

In Concept III, there are four possible types of delay, i.e., the input transmission delay between real-time simulators and sensors, the output transmission delay between real-time simulators and power amplifiers, the computational delay caused by digital controllers, and the modulation delay caused by PWM modulation if a SMPA is employed. These extra delays will change the equivalent impedance of the emulated machine. Thus, the stability of the system will be affected. The current or the voltage will oscillate due to the instability [54], which threatens the safety of experimenters and facilities and leads to unreliable results. Guillo-Sansano *et al.* [54] point out that even for the same PHILS system, the total delays may be variable. Thus, the system may switch between stable and unstable conditions. Besides, protections should be triggered under certain circumstances, such as overcurrent induced by faulted converter under test, and LPAs are easier to be damaged by overheating than SMPAS.

In Concept IV, PEBE, fewer delays are introduced because the characteristics are implemented in the converter controller. The electric machine is modeled as an individual model, which is different from the network model in HILS. Besides, due to the control process of the digital processor, the total time delay of the system is fixed [55]. So, the stability of Concept IV is better than that of Concept III. Like Concept III adopting SMPAs, PEBE can adapt to the failures of the converter under test under the premise of safety.

For Concept III and Concept IV, the dynamics of power amplifiers and emulating converters will also affect the stability. Various factors, such as modulation delays, passive filters, and dead time, make the dynamic characteristics of power amplifiers nonideal. These coupled dynamics and interactions may induce instability. Wang and Blaabjerg [57] illustrate the details about modeling and stability analysis of coupled converters. Ma *et al.* [58] give a detailed investigation into the modeling and stability analysis of two converters coupled by different filters.

C. Power Level, Testing Efficiency, and Cost

The power level, test efficiency, and total cost of the test bench of different concepts are important factors affecting their suitability.

The power level of Concept I is determined by the electric machine under test, which ranges from several Watts to Mega Watts [59], [60]. In Concept II, there are only signals transmitted between the drive controller and the real-time simulator. So, Concept II is the signal-level simulation. The power level of Concept III depends on the types of power amplifiers. For PHILS adopting LPAs, the power level is relatively lower than that of PHILS adopting SMPAs because LPAs work in amplifying-mode, leading to higher voltage drop and higher power loss [47]. For PHILS adopting SMPAs and Concept IV, the power level depends on the topologies and the devices used. Typically, a two-level converter is adopted due to its simplicity. PHILS adopting SMPAs and Concept IV can adopt multilevel converters, such as modular multilevel converters, to achieve higher power level [59]. Generally, the power level of SMPAs can be much higher than that of LPAs.

The test efficiency of Concept I is determined by the energy consumed by the electric machine and the load machine. The consumed energy is converted into kinetic energy and heat. For Concept II, the consumed energy is used to power the drive controller and the real-time simulator, which is much lower than the energy consumed in other concepts. For Concept III and Concept IV, the testing efficiency of LPAs is much lower than that of SMPAs on the similar power level because of the different working modes [61]. Compared with Concept I, the energy consumed in Concept III adopting SMPAs and Concept IV can be much lower on the similar emulation capability. The energy consumed in these two concepts can be the total power loss of SMPAs and the drive converters. Without the real-time simulator, the test efficiency of Concept IV is slightly higher than that of Concept III adopting SMPAs.

The cost of Concept I is very expensive because of the actual electric machine and load machine. These physical facilities are more expensive than power amplifiers and converters in Concept III and Concept IV. In Concept II, the real-time simulator costs more than other facilities, but the lack of power amplifiers make Concept II cheaper than Concept III. The cost of Concept III is much higher than the cost of Concept IV because of the presence of the real-time simulator. PHILS adopting LPAs is usually more expensive than PHILS adopting SMPAs at the similar capability. The total cost of Concept IV is the lowest among these four concepts because of the absence of real-time simulators and actual machines.

D. Suitable Testing Scenarios

With extra facilities, all the four concepts can emulate the desired environmental conditions and validate the reliability concerning temperature and humidity. The differences of suitable testing scenarios mainly lie on other factors.

With actual facilities, Concept I can emulate the mechanical behaviors, control strategies, and nonideal electromagnetic properties, but this type of emulation is not flexible. It is very difficult to test the drive system under faulted conditions and overload conditions, which may threaten the safety of experimenters and damage the electric machines. Due to the low bandwidth limited by the mechanical inertia, Dyno test is mostly performed under steady state or low dynamic process. Durability of the drive converter and the electric machine can be validated in this concept.

In Concept II, the control algorithm can be tested when it is programmed on the controller. Due to the flexibility of real-time simulators, various functions and control strategies can be validated under almost all the mission profiles. However, the lack of high-power stage limits the scope of this concept, e.g., durability validation of the drive converter.

TABLE I
BENCHMARK OF DIFFERENT DRIVE TESTING CONCEPTS

Concept / Characteristics		I: Dyno test	II: CHILS	III: PHILS adopting LPA	III: PHILS adopting SMPA	IV: PEBE
Band width	**Limits**	Mechanical inertia of the machine and load.	Discrete time of real-time simulators, time step of signal interface modules.	Bandwidth of power amplifier.	Bandwidth of power amplifier.	Bandwidth of emulating converter.
	Ranking	Lowest	Highest	Higher	High	High
	Typical number	A few hundred Hz [16], [17]	Hundred kHz to several MHz [41], [53]	50kHz (LPA) [47]	up to several kHz (SMPA) [48] –[52]	5kHz [62]
Stability issues		Mechanical system stability, inertia mismatch, torque mismatch	Control strategies, stability of the real-time simulator.	Interface algorithm, dynamic characteristics of power amplifier, stability of coupling elements	Interface algorithm, dynamic characteristics of power amplifier, stability of coupling elements	Dynamic characteristics of emulating converter, stability of coupling elements
Types of extra delays		No	Computational delay, transmission delay. Unfixed	Computational delay, transmission delay. Unfixed.	Computational delay, transmission delay, modulation delay. Unfixed.	Modulation delay, computational delay. Fixed
Robustness to faulted CUT		Lowest	Highest	High	Higher	Higher
Power level		High	Signal level	Low	High	High
Test efficiency		Lowest	Highest	Low	High	Higher
Test bench cost		Highest	High	Higher	Higher	Lowest
Suitable testing scenarios		Steady state test or low dynamic test	Validations of control strategies.	Low-capacity test	High-capacity test	High-capacity and high-dynamic test
Testing targets		Durability of the machine drive, Durability of the electric machine, functions of control strategies.	Functions of control strategies.	Performance and stability of the machine drive, performance and stability of control strategies.	Performance and stability of the machine drive, performance and stability of control strategies.	Performance, stability, and reliability of the machine drive, Performance, stability, and reliability of control strategies.

Concept III can be performed at real power level. Nonideal characteristics related to the power stage and the power electronic converter are included. Thus, a realistic testing environment can be created. Due to the flexibility of the real-time simulator, Concept III can almost emulate all the possible characteristics. Experiments and tests involving risks or hard to be performed in actual drive systems can be easily implemented in PHILS [19]. However, the unfixed system delay may make the system switch between stable and unstable conditions [54]. It is difficult to reproduce abnormal conditions of high bandwidth in this concept. So, Concept III can validate the performance and stability of the drive converter and control strategies.

Fewer types of extra delays and flexible control of emulating converters make Concept IV a suitable approach to test the electric machine drive systems within wider frequency ranges. The Concept IV provides the realistic environments for the drive system with fewer stability issues and higher bandwidth. Concept IV can present almost all the characteristics with minimal risk. So, Concept IV can be adopted to validate the performance, stability, and reliability of the drive converter and control strategies even under abnormal conditions.

E. Benchmark of Concepts

First, an ideal mission profile emulation system needs to accurately recreate the key factors of the electric machine, so the tests of the drive converter can be performed close to actual conditions. Second, complicated mission profiles must be reproduced safely and stably to protect the operators. Then, the emulation system should be flexible and free to program, thus different mission profiles can be recreated for different testing targets. Finally, the testing system should be efficient and cost-effective. Based on these aspects, a comparison is presented in Table I to summarize the characteristics of these concepts, and to distinguish the most promising one.

Concept I can reflect the mechanical and control characteristics of the emulated machine because a real electric machine is used in the testing system. However, the low dynamics and high mechanical inertia prevents Concept I from the testing of high dynamics. Besides, the two physical machines make the whole system bulky, expensive, and the least robust.

Concept II involves no power facility, so non-ideal factors related to high power stage will not be considered, leading to robust testing system but unconvincing testing results. However,

for the testing and improvement of control algorithm, Concept II has a great advantage.

Concept III raises the power level to the actual level with the power amplifier, which introduces the non-ideal factors, e.g., sampling noises. However, the extra delays and high cost of the real-time simulator prevent Concept III from being widely used. Besides, Concept III adopting LPAs is less robust than Concept III adopting SMPAs.

Concept IV shares the strengths of Concept III, and it has a fixed delay, which means that stability issues are easier to be dealt with. Meanwhile, the robustness of Concept IV is similar to that of Concept III adopting SMPAS. Without the real-time simulator, Concept IV can be achieved at a very low cost. So, Concept IV is the most promising testing method of the electric machine drive system and the next chapters will focus on the features of Concept IV.

IV. Features of Power-Electronics-Based Emulation (Concept IV)

The PEBE can be realized in different ways in order to achieve desired results according to the testing scenarios. The differences between these methods include coupling with converter under test, types of machine models implemented in converter controllers, and control system.

A. Coupling With Converter Under Test

As it is shown in Fig. 1, signals transmitted between the drive controller and the electric machine are electrical signals sampled by sensors and mechanical signals generated by encoder/resolver. According to the degrees of coupling between the electric machine drive and the machine emulator, the PEBE can be divided into two types: PEBE without signal transmission and PEBE with signal transmission.

The PEBE without signal transmission is shown in Fig. 4(a). In essence, the PEBE without signal transmission has the same interfaces compared with the actual machine. The actual machine can be replaced by the emulator without any change on the drive system. In this case, the voltage/current is still sampled by sensors, but the signals related to the rotor speed are generated by encoder/resolver pulse generators. A low-pass voltage filter is needed because the voltage produced by the converter under test is in the form of irregular PWM waveforms, which will distort the frequency response of PEBE in a high-frequency band [56].

The PEBE with signal transmission is shown in Fig. 4(b). In this case, the signals can be directly transmitted between the drive controller and the emulating controller with extremely low delay. Besides, the low-pass voltage sampling is removed. Thus, more details are reserved, and the bandwidth of the entire system is enhanced [56]. This structure enables the tests at smaller timescales and enhances the accuracy of tests without plug-and-play requirements.

B. Electric Machine Model

The electric machine model implemented in PEBE can be divided into current-response model and voltage-response model,

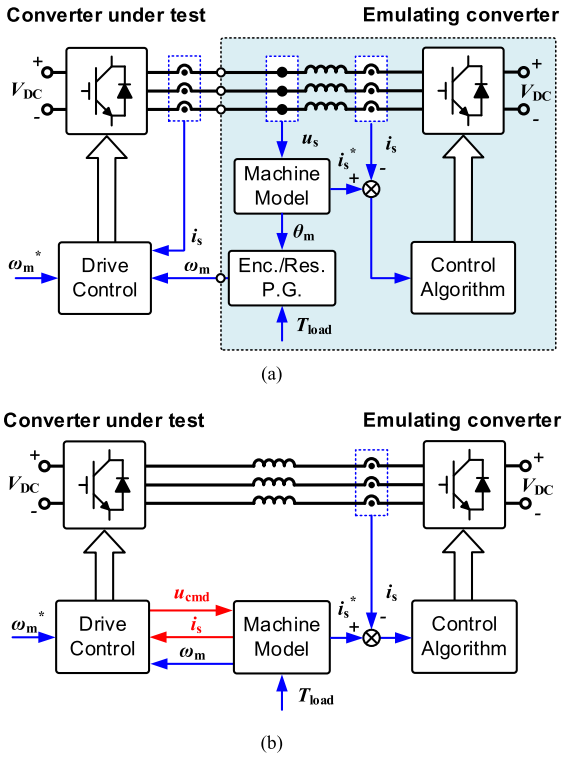

Fig. 4. Power-electronics-based emulation with varying degrees of coupling. (a) PEBE without signal transmission. (b) PEBE with signal transmission. Enc.: Encoder. Res.: Resolver. P.G.: Pulse generator.

based on the output of the machine model. For the current-response model, the voltage is needed to calculate the current reference. And for the voltage-response model, the value of current is needed.

Up until now, there are two methods to extract the current-response model of an electric machine. One is the simplified mathematical model. The undesired characteristics of a real machine are not concerned in the simplified model, such as saturation effects, slot harmonics, torque ripples, and so on. This model trades the accuracy for lower demand for computational resources. The simplified model is programmed in the emulating controller as math equations. Equations (1)–(3) are a simplified model of a PMSM in the *dq*-frame [63]–[65]. Equation (1) represents the relationship between the terminal voltage and current of the stator. Equation (2) is the equation of torque, and Equation (3) is the equation of motion

$$\begin{cases} u_{\mathrm{d}} = R_{\mathrm{s}} i_{\mathrm{d}} + L_{\mathrm{d}} \frac{\mathrm{d}i_{\mathrm{d}}}{\mathrm{d}t} - \omega_{\mathrm{e}} L_{\mathrm{q}} i_{\mathrm{q}} \\ u_{\mathrm{q}} = R_{\mathrm{s}} i_{\mathrm{q}} + L_{\mathrm{q}} \frac{\mathrm{d}i_{\mathrm{q}}}{\mathrm{d}t} + \omega_{\mathrm{e}} L_{\mathrm{d}} i_{\mathrm{d}} + \omega_{\mathrm{e}} \psi_{\mathrm{f}} \end{cases} \tag{1}$$

$$T_{\mathrm{e}} = \frac{3}{2} p_{\mathrm{n}} [\psi_{\mathrm{f}} i_{\mathrm{q}} + (L_{\mathrm{d}} - L_{\mathrm{q}}) i_{\mathrm{d}} i_{\mathrm{q}}] \tag{2}$$

$$T_{\mathrm{e}} = T_{\mathrm{load}} + J \frac{\mathrm{d}}{\mathrm{d}t} \omega_{\mathrm{m}} + F \omega_{\mathrm{m}} \tag{3}$$

where R_{s}, L_{d}, and L_{q} represent the equivalent resistance and inductance on the *dq*-axis, respectively, u_{d}, u_{q}, i_{d}, and i_{q} are the terminal voltage and stator current on the *dq*-axis, respectively, ψ_{f} is the flux linkage of the electric machine, ω_{m} and ω_{e} are the mechanical angular frequency and electromagnetic angular

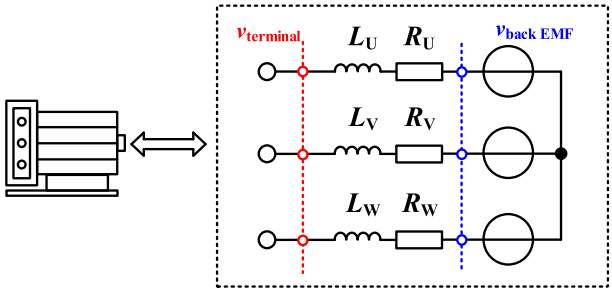

Fig. 5. Terminal voltage and back EMF for emulation of the electric machine.

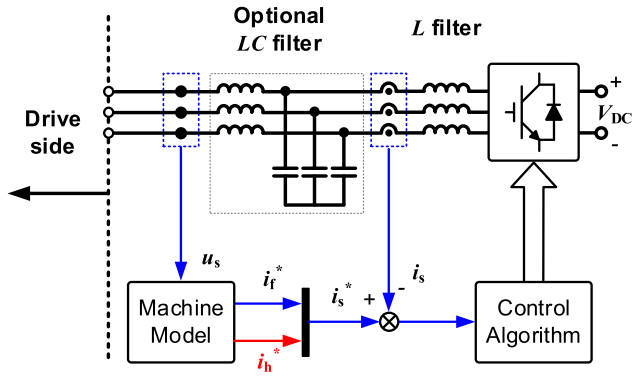

Fig. 6. Closed-loop current control. i_f^*: fundamental component. i_h^*: harmonics.

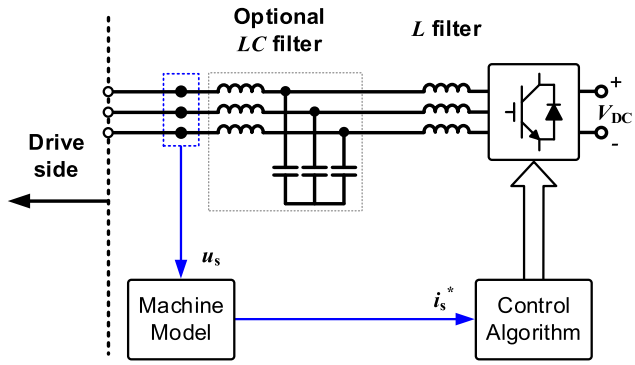

Fig. 7. Open-loop current control.

frequency of the electric machine, respectively, and T_e, T_{load}, p_n, F, and J are the electromagnetic torque, load torque, numbers of pole pairs, coefficient of viscous friction, and inertia of the electric machine, respectively.

The other one is the finite element method (FEM) based model known as the detailed FEM model. The detailed FEM model can be obtained from FEM software or imported from machine design tools. Electric machine parametric variations are usually stored in lookup tables [41], [66]. With this detailed machine model, almost all the machine behaviors can be emulated accurately, but this type of model requires high computational resources. Masadeh *et al.* [67] introduce an approach to extract the nonideal parameters of the electric machine, and these parameters are applied to the simplified mathematical model. This method can obtain much more accurate results than the simplified model with lower demand for computational capability.

The voltage-response model is usually converted from the simplified mathematical model of current-response mode, which means the voltage-response model is not accurate but simple [68]. The calculated voltage reference can be the back electromotive force (EMF) of the machine or its terminal voltage as it is illustrated in Fig. 5. The emulation of the back EMF requires a coupling inductance at the value of the average inductance of the electric machine to precisely recreate the desired current. However, the average inductance of the electric machine is usually quite large, and it is not so practical. So, the emulation of the terminal voltage is usually adopted in PEBE [69].

These types of the machine model have their own application scenarios. The simplified mathematical model is sufficient for the durability test of the power electronic converter and other tests with lower requirement of the accuracy. The detailed FEM model is necessary when the tests involve the control strategies or the accuracy is important, such as physical-fault conditions. The voltage-response model has a lower emulation fidelity, but it is acceptable for durability test of the drive converter or high-speed machine emulation with the need of higher bandwidth.

C. Control System

The control system of PEBE can be divided into current control mode and voltage control mode according to the characteristics of controlled electric quantities.

A current-response model is naturally adopted in current control mode, and closed-loop current control is usually used to ensure the emulation accuracy. The configuration of the closed-loop current control is shown in Fig. 6. The most used current controller is the proportional–integral (PI) controller. Using Park transformation, ac components in three-phase stationary frame can be transformed into dc components in the synchronous *dq*-frame. Then, the reference current can be tracked without static error. However, the closed loop of current control behaves like a low-pass filter in the frequency domain. In this case, the characteristics of current and voltage at high frequency will be distorted [68], [70]. Typically, the drive converter also works in current control mode. To avoid conflicts between these two current control loops, the bandwidth of the emulating current controller needs to be at least five times more than the bandwidth of the drive controller [71]. To regulate the harmonics, as it is highlighted in Fig. 6, the proportional–resonant (PR) controllers can be adopted. Typically, the fundamental component is controlled by a PI controller, while the harmonics are controlled by PR controllers. This control structure can be used to emulate the fault situation [40], [72] or to suppress the zero-sequence harmonics [59], [73].

Besides the closed-loop current control, the open-loop current control can also be adopted, as shown in Fig. 7. In this case, the current reference is directly sent into the controller, and then is multiplied by the filter impedance. Thus, the converter can

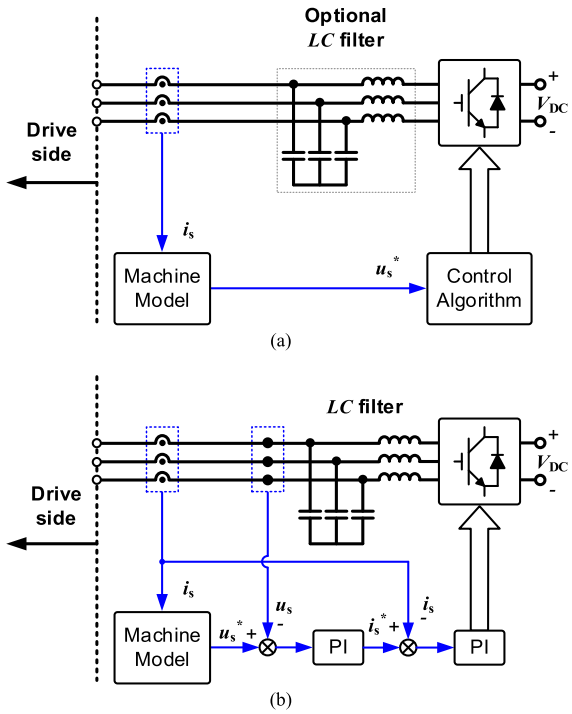

Fig. 8. Voltage control structure. (a) Open-loop voltage control. (b) Closed-loop voltage control.

track the current reference. Without the closed current control loop, the emulation bandwidth is enhanced, but the accuracy is compromised.

For voltage-control mode, an open-loop control is usually adopted and Fig. 8(a) illustrates the control structure of open-loop voltage control [69]. In this case, the conflicts between the two closed current control loops no longer exist, and the emulation bandwidth is enhanced. However, voltage control mode can only be implemented when the emulation accuracy is not important because the detailed FEM model is not available [68].

When *LC* filters are adopted, it is better to adopt closed-loop voltage control, and the configuration is shown in Fig. 8(b). With the double-loop PI controller, *LC* filters will be decoupled from the perspective of *dq*-frame. Thus, better dynamic performance can be obtained, and the static error induced by deadtime can be reduced. In this case, the emulation bandwidth is still limited by these control loops.

V. Challenges of Power-Electronics-Based Emulation

There are several challenges when implementing PEBE, such as limited bandwidth, control coupling, stability, power supply, and mismatch in the switching frequency and carried phase angle, which are discussed in the following sections.

A. Bandwidth Limitation

The bandwidth of PEBE is limited by multiple factors, such as the passive filters, the control dynamics, and the power amplifiers. A lower bandwidth will lead to inaccurate test results, especially in transient conditions.

L [40], [41] and *LCL* [74], [75] filters have been reported in the electric machine emulation in current-response mode, and *LC* [69] filters have been reported in the electric machine emulation in voltage-response mode. *LCL* and *LC* filters both suppress high-frequency components effectively, but the dynamics of the high frequency are also affected. To extend the bandwidth, the *L* filter is the most preferable coupling element according to the research and analysis [40], [41], [68], [71].

To achieve a higher bandwidth, control algorithms of better dynamic performance have been adopted [40], [76], [77]. Amitkumar *et al.* [40] employ PR controllers to guarantee the amplitude of specific frequency components, and Luo *et al.* [76] and Rao and Chandorkar [77] employ a model-predictive-control controller to extend the control bandwidth. These control algorithms increase the burden on the processors, and may lead to higher risk of instability.

It is proposed in [70] that the closed-loop current control can be substituted with an open-loop control. This direct impedance regulation (DIR) method combines the accuracy of the current-response model with the high bandwidth of voltage-control mode. The configuration of PEBE based on DIR is shown in Fig. 9(a), with the bode diagram in Fig. 9(b). The characteristics of the emulator based on DIR become much closer to the actual machine compared with the emulator based on closed-loop current control (CLCC). The DIR can eliminate the impact of CLCC in middle frequency band, but the deviation still exists in the high-frequency band. This deviation is mainly induced by the low-pass voltage sampling and other delay links, which is neglectable in most cases [70].

The experimental results shown in Fig. 10 also demonstrate the superiority of DIR. The system parameters are in [70], and the mission profile adopted here is as follows: the rotational speed is set as 60 r/min at first in order to simulate the soft start of the target electric machine. At 3 s, the electric machine is accelerated to its rated maximum speed (3900 r/min) within 4 s, where the fundamental electrical frequency is 260 Hz. The load torque is 1 N·m and has no step.

The emulator based on CLCC goes unstable and triggers overcurrent protection when accelerated to 6.2 s. While for the emulator based on DIR, it can be accelerated to the maximum speed without any instability.

The major challenge for DIR is that the emulation accuracy will be directly affected by the variations of the inductance parameters.

Another way to enhance the emulation bandwidth is to increase the bandwidth of the power amplifier, which can be realized by adjusting the topology of the amplifiers or improving the performance of the devices. Amitkumar *et al.* [68] use linear amplifiers as power amplifiers, and the bandwidth of linear amplifiers can reach dozens of kilo Hertz. However, linear amplifiers are not suitable for high-power applications, and other drawbacks, such as high costs and weight, restrict the use of linear amplifiers. Grubic *et al.* [78] employ the linear inverters (LinVerter) as power amplifiers because of the satisfactory output characteristics. However, LinVerter is constructed with lots of power electronics devices in a complicated method, which prevents it from being widely used [67]. The work in [62], [76],

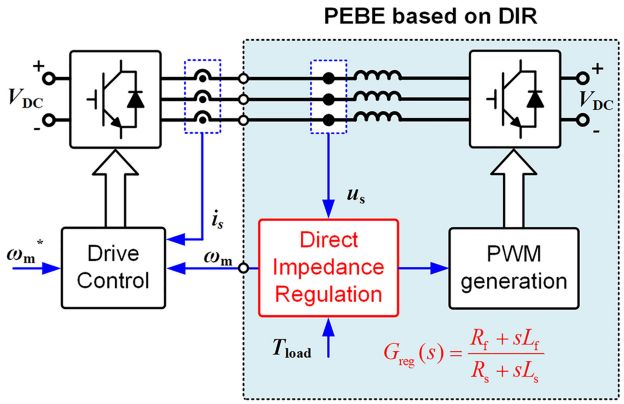

(a)

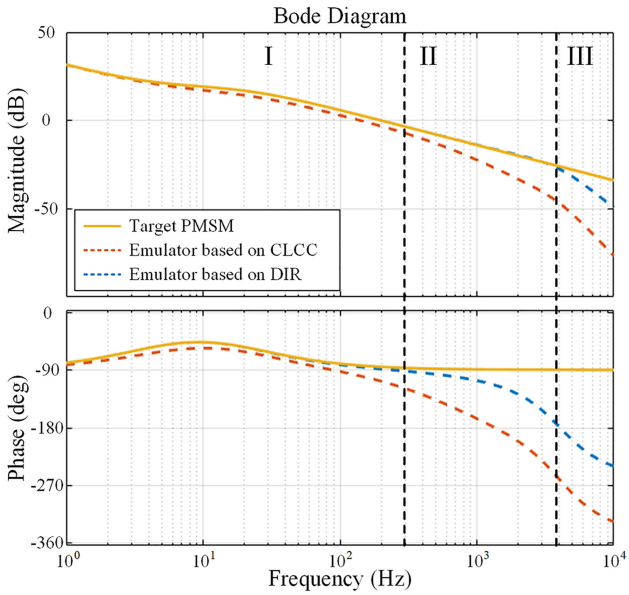

(b)

Fig. 9. Electric machine emulation based on direct impedance regulation. (a) Circuit configuration. (b) Bode diagram.

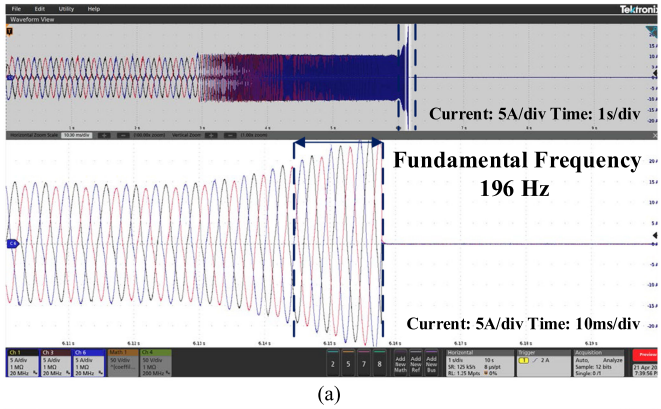

(a)

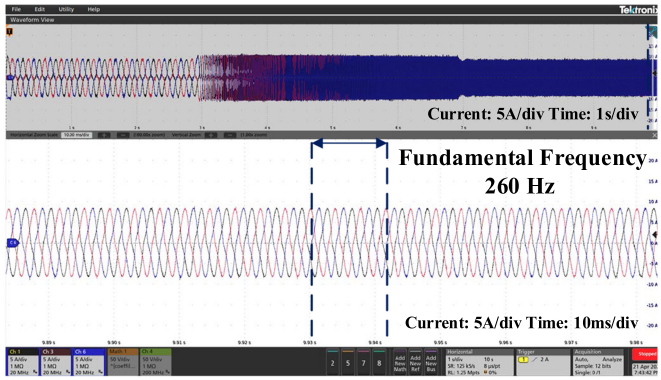

(b)

Fig. 10. Experimental results. (a) Electrical responses of the typical emulator based on CLCC. (b) Electrical responses of the proposed emulator based on DIR.

and [79] enhance the control bandwidth with the application of silicon carbide (SiC) based MOSFET, but the limitations of wide bandgap devices in power level and cost prevent them from being widely used. Paralleled or interleaved converters are also adopted in [79] and [80] to achieve a higher equivalent switching frequency, but the current sharing problems between multiple converters need to be further discussed.

B. Control Coupling and Stability

Although *L* filter is widely adopted because of its high bandwidth and easy control, *LC*/*LCL* filters are more often used due to the better characteristics in the frequency domain and less error they produce [77], [81]. Besides, the implementation of *LC*/*LCL* filters introduces neutral point into the emulation system, which makes the emulation of unsymmetrical conditions easier. However, the implementation of *LC*/*LCL* filters may bring unexpected system resonance and control coupling [58].

Fig. 11(a) shows a typical three-phase interconnected converter system, where a voltage-controlled converter with *LC* filters is connected to a current-controlled converter with *LCL* filters. Ma *et al.* [58] analyze the mechanism of unexpected system resonance and control coupling in this system. Fig. 11(b) shows the block diagram of the system in Fig. 11(a), together with the control loops based on the filter impedance network. The matrix for the closed-loop transfer functions of the interconnected converter system considering filter impedances and control loops is given as follows:

$$\begin{bmatrix} v_{\mathrm{PCC}}(\mathrm{s}) \\ i_{\mathrm{PCC}}(\mathrm{s}) \end{bmatrix} = \begin{bmatrix} \frac{G_A(\mathrm{s})}{1+G_B(\mathrm{s})\cdot G_D(\mathrm{s})} & \frac{G_B(\mathrm{s})\cdot G_C(\mathrm{s})}{1+G_B(\mathrm{s})\cdot G_D(\mathrm{s})} \\ \frac{-G_A(\mathrm{s})G_D(\mathrm{s})}{1+G_B(\mathrm{s})\cdot G_D(\mathrm{s})} & \frac{G_C(\mathrm{s})}{1+G_B(\mathrm{s})\cdot G_D(\mathrm{s})} \end{bmatrix} \cdot \begin{bmatrix} v_{\mathrm{ref}}(\mathrm{s}) \\ i_{\mathrm{ref}}(\mathrm{s}) \end{bmatrix} \quad (4)$$

where v_{PCC}, i_{PCC}, v_{ref}, and i_{ref} are the PCC voltage, PCC current, the voltage reference and the current reference, respectively. Definitions of G_A, G_B, G_C, and G_D can be found in [58].

Fig. 12 shows the bode diagrams of external impedances of voltage-controlled converter and current-controlled converter, together with an inductive grid impedance (15 mH) in order to trigger the instability of the current-controlled converter. The system parameters are in [58]. Different from the typical resonance in grid-connected converter system (hundreds of Hz), the

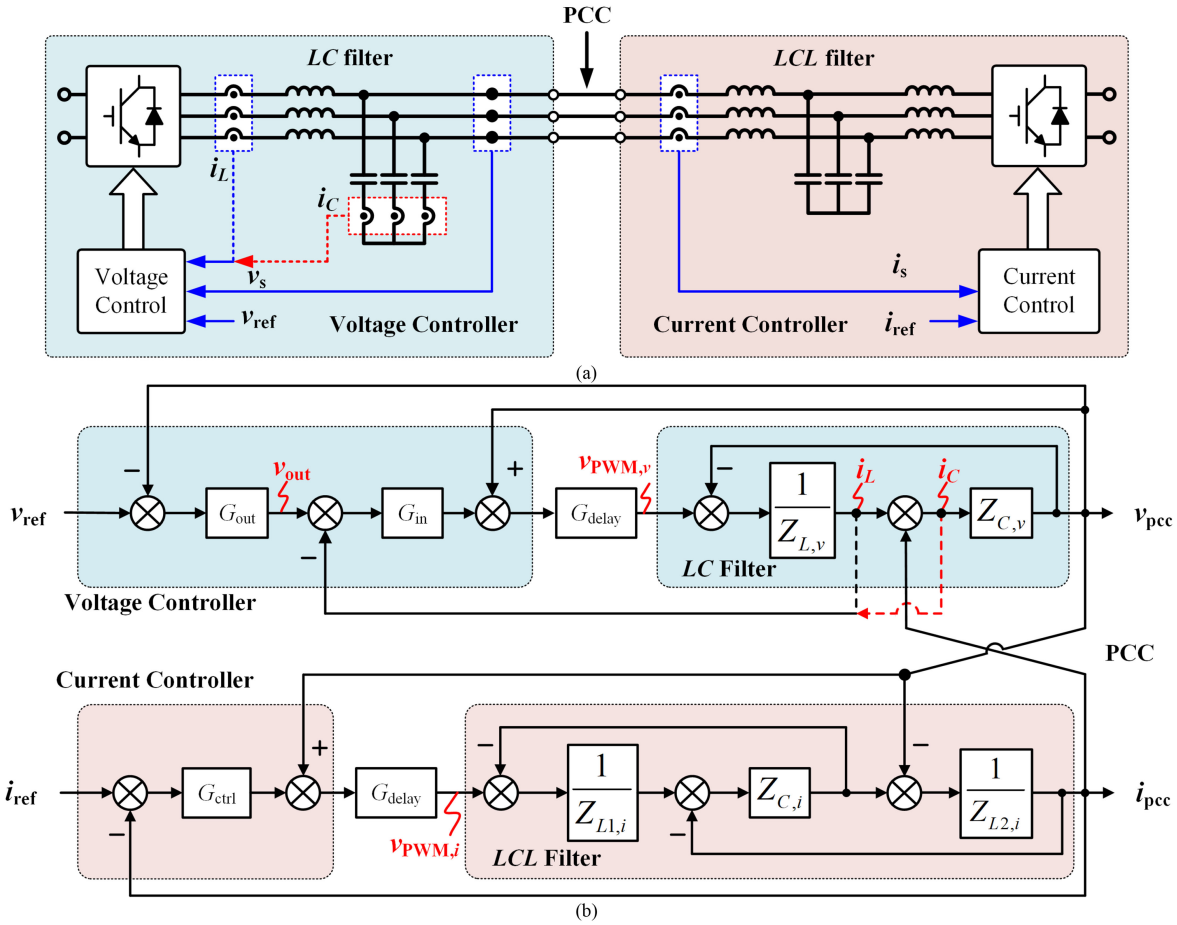

Fig. 11. Connected converters system. (a) Voltage-controlled converter with *LC* filter connected to current-controlled converter with *LCL* filter. (b) Block diagram of the system with voltage-controlled and current-controlled converters connected in parallel. PCC: point of common coupling.

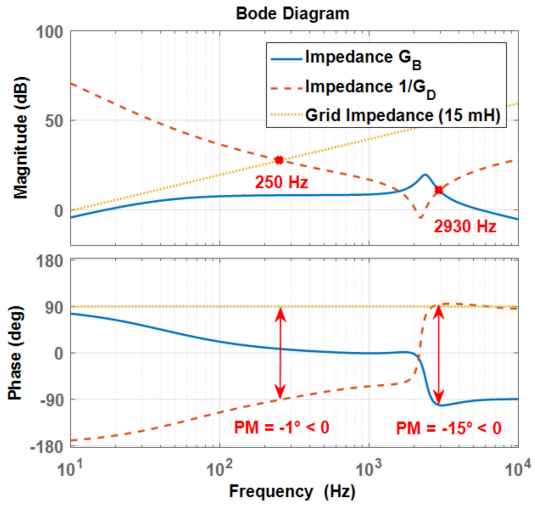

Fig. 12. Bode diagrams of output impedances of voltage-controlled converter G_B and current-controlled converter $1/G_D$. The grid impedance equals 15 mH.

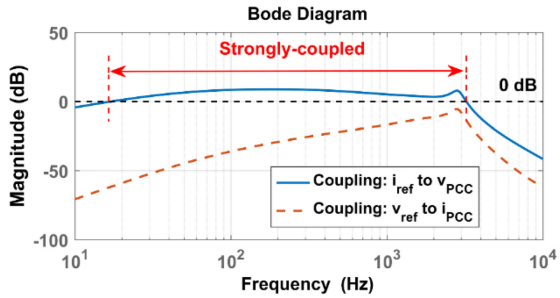

Fig. 13. Magnitude–frequency curves of coupling terms $v_{\mathrm{PCC}}/i_{\mathrm{ref}}$ and $i_{\mathrm{PCC}}/v_{\mathrm{ref}}$ when inductor current i_L is fed forward for active damping.

resonance in this system can be triggered at a higher frequency (several kHz).

On the other hand, the coupling from current reference to PCC voltage is strong in both low-frequency band and mid-frequency band, which can be seen from the bode diagram shown in Fig. 13. The PCC voltage v_{PCC} will be apparently distorted if errors or distortions are introduced into the current reference.

Potential solutions of resonance and coupling issues in the interconnected converter system have also been discussed in [58]. For resonance issues, passive damping methods, such as inserting a simple resistor into capacitor branch, can effectively

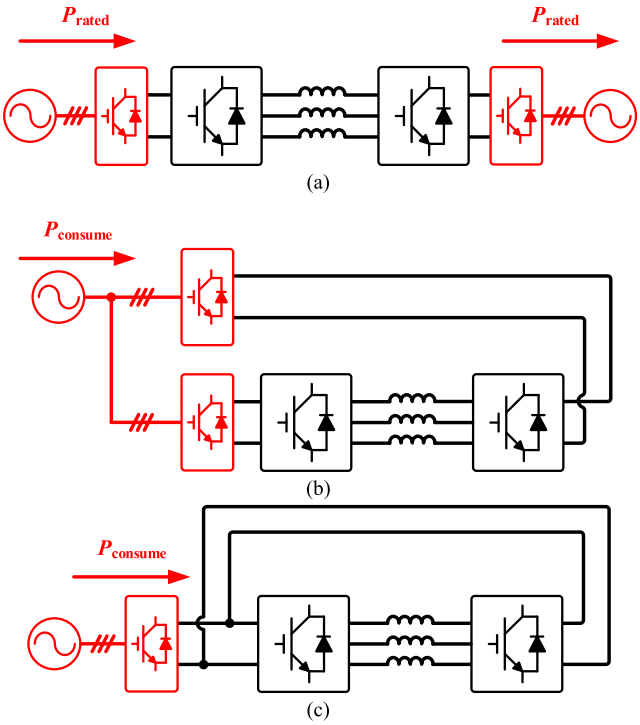

Fig. 14. Power supply solutions for electric machine emulation system. (a) Converters powered by separate power sources. (b) Converters powered by common ac power source. (c) Converters powered by common dc power source.

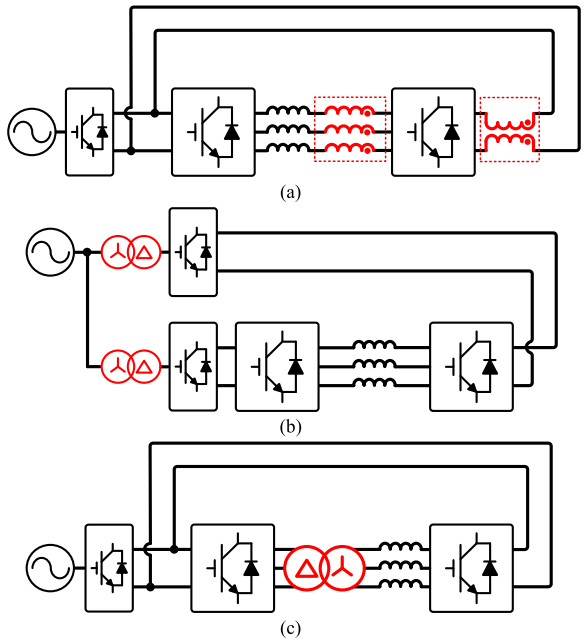

Fig. 15. Solutions to eliminate zero-sequence current. (a) Based on common-mode inductor. (b) Based on transformers located between ac source and rectifiers. (c) Based on transformer located between two converters.

stabilize the system. For coupling issues, feeding forward the capacitor current of *LC* filter can realize decoupling of current reference and PCC voltage in low-frequency band. In mid-frequency band, adding differential terms into feedforward path is a commonly seen approach.

C. Power Supply

As it is shown in Fig. 14(a), the machine drive converter and the emulating converter are powered by individual power source. In this case, no circulating path for zero-sequence current exists, and the power is not able to circulate among the system. Thus, more power is consumed in this system, and the capacity of the power sources must be at the same or even higher level than the emulation system.

The machine drive converter and the emulating converter sharing a common power supply is shown in Fig. 14(b) and (c). In Fig. 14(b), the two converters are powered by a common ac power supply, and in Fig. 14(c), the two converters are powered by a common dc power supply. In both cases, the power flow is circulated among the system, and the power source only needs to provide the power loss in the testing system. However, for the situation shown in Fig. 14(b), the two rectifiers must be at the same or higher power level than the emulation system. Meanwhile, there are zero-sequence circulating paths among different modules. Thus, undesired harmonics and extra loss will be introduced.

Different methods have been proposed to eliminate the circulating currents. First, a common-mode inductor can be implemented as it is shown in Fig. 15(a) [59]. Typically, either ac chokes or dc chokes are assigned. Second, a transformer whose secondary side adopts delta connection can be placed between the ac power source and the rectifier [82], as it is shown in Fig. 15(b). While a transformer whose primary side adopts delta connection can be placed between the drive converter and the emulating converter [73], [75] as it is shown in Fig. 15(c). The third way is realized by adding a PR-based control loop to reduce the amplitude of zero-sequence current [59]. The first way is hard to achieve because the value of the common-mode inductor is impossible to be infinite, so the first way is generally used in conjunction with the third method [59]. The second method is available when the system is powered by a common ac source, and the transformers are placed between the ac power source and the rectifier. If the transformer is placed on the ac side between the drive converter and the emulating converter, there is no requirement of ac power sources. In this case, the zero-sequence current can be eliminated and the transformer tap position can be adjusted according to different power requirements. However, the bandwidth of the testing system will be narrowed, and the capacity of the transformers and the rectifiers must be at the same or even higher level than the emulation system. The PR controllers in the third way consumes a lot of computational time, and the fundamental frequency in the electric machine drive system is undetermined, which makes the implementation of the PR-based controller more complicated.

The methods mentioned above insert transformers or inductors into the circuit to block the zero-sequence path, while the nonlinear characteristics and saturation characteristics may

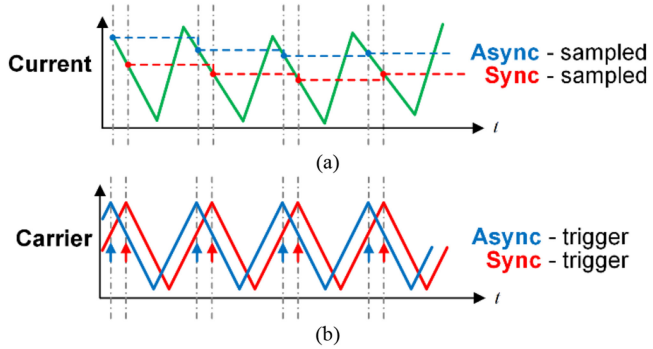

Fig. 16. Illustration of sampling distortion. (a) Sampled results. (b) Synchronous sampling and asynchronous sampling.

induce instability, and distort the characteristics in the frequency domain. More advanced methods are needed to eliminate the common mode current.

D. Mismatch in Switching Frequency and Carried Phase Angle

In a PEBE-based electric machine emulation, the carriers of the controllers may be of the same frequency and different phases, or different frequencies. This mismatch in frequency and carried phase angle may introduce common mode ripples among the converters, and these ripples will distort the sampled results.

Fig. 16 shows the current sampled results and the carriers when the carriers have the same frequency but different phases. The solid line represents the ideal condition where the two carriers have the same frequency and phase. In this case, the current value is sampled when the carrier reaches the highest or the lowest point and the sampled value is just in the middle point of the ripples. As it is shown in Fig. 16(a), the sampled current curve (marked in red) does not have a dc offset and the input value of the ADC is equivalent to the average value over one switching period. However, if the two carriers have a phase difference, the sampling point will deviate from the normal position as it is shown in Fig. 16(b) marked in blue. Thus, an offset is introduced to the sampled current curve (marked in blue) as it is shown in Fig. 16(a). So, the sampled results will be distorted when the two carriers have the same frequency but different phases. The sampled results are similar when the two carriers have different frequencies. The distorted sampled results will introduce unexpected harmonics, and make the testing results untrustworthy.

Fig. 17 illustrates the analog-to-digital conversion of the sampled current. The current of the inductor, i_s, is sampled by current sensor and converted to current signal, i_1. Then, i_1 is converted to i_{sampled} by pulse sampling.

When the two carriers have mismatched frequencies, harmonics of beat frequency will be introduced in the sampled signal. When two carriers have the same frequency but different angle, a dc offset and low-frequency harmonics will appear in the current

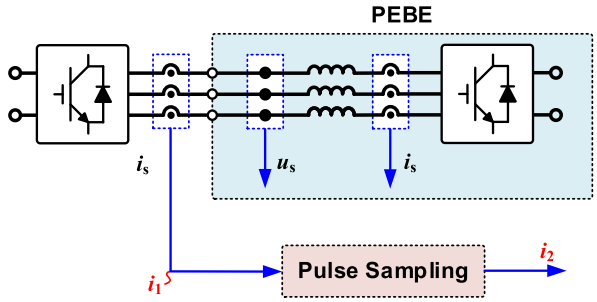

Fig. 17. Analog-to-digital conversion.

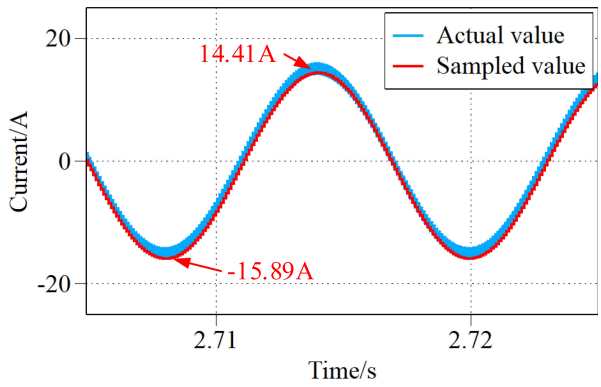

Fig. 18. Waveforms of inductor current when two carriers have the same frequency but mismatched phase. Switching frequency = 10 kHz. Phase difference of carriers = 90°.

sampled signal, which can be derived from the following:

$$i_2^*(\mathrm{j}\omega) = \frac{1}{T_{\text{sampling}}} \sum_{q=-\infty}^{\infty} i_1(\mathrm{j}\omega_{\text{in}} - q \cdot \mathrm{j}\omega_{\text{sampling}}) \quad (5)$$

where ω_{in} represents the angular frequency of the current, ω_{sampling} represents the angular frequency of sampling, T_{sampling} represents the sampling period, and q is an integer.

This has been proved through simulations as illustrated in Figs. 18 and 19. The circuit is built as it is shown in Fig. 3(d). The inductance is 2.5 mH, and the parasitic resistance is 0.64 Ω.

Fig. 18 shows the actual waveform of the inductor current and the sampled waveform when the two carriers have the same switching frequency but a mismatch in phase angle. As it is shown in Fig. 18, unexpected dc offset is introduced to the sampled results but it does not exist in the actual current waveform.

Fig. 19(a) shows the actual waveform and the sampled current waveform when the two carriers have mismatched switching frequencies. As it is shown in Fig. 19(a), unexpected harmonics are introduced to the sampled results, and a frequency analysis is shown in Fig. 19(b). The actual current contains the spectrum components of the switching frequencies (9 and 10 kHz). While for the value sampled by the emulating converter, the spectrum component of beat frequency (1 kHz) is introduced.

This distortion only exists in the sampled signals, which means there is a difference between the actual current and

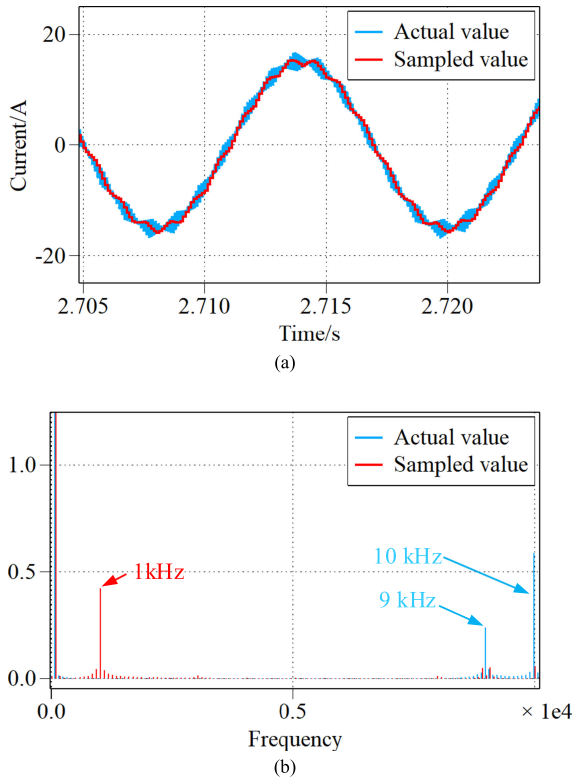

Fig. 19. Waveforms of the inductor current when the switching frequencies are mismatched. (a) Inductor current waveforms. (b) Frequency spectrum of inductor current and sampled value. Switching frequency of drive converter = 9 kHz. Switching frequency of emulating converter = 10 kHz.

the sampled current. In this case, control distortion may occur due to this sampling error, and the actual waveform will be distorted due to the control distortion. The sampling error can be avoided by implementing anti-aliasing filter. However, for the electric machine drive system, the anti-aliasing filters do not necessarily exist. Besides, these high-order current ripples will lead to increased power losses and compromised reliability of the dc-link capacitors [83], [84]. Further discussion and advanced methods are needed to avoid the sampling errors.

VI. Conclusion

With the widespread use of electric machines, the stability and reliability of the drive systems become vital. More advanced testing methods are urgently needed. In this article, key factors of machine drive systems to be emulated are clarified, and various testing methods have been developed. Up until now, four concepts of electric machine emulation have been discussed. The PEBE has been considered as the most promising method due to its flexibility, high power level, low cost, and so on. Different configurations and features of PEBE have been introduced and they can be selected according to the testing requirements.

However, there are still several challenges needed to be solved, including the limited bandwidth, control coupling, stability issues, power supply, and the mismatching in switching frequency and carrier phase angle. Some solutions have also been introduced but the results are not satisfactory enough. The PEBE with signal transmission can realize full-bandwidth emulation with certain methods but is not plug-and-play, which limits its usage scenarios. Eliminating the zero-sequence current by inserting common mode choke will bring extra nonlinear characteristics into the system. Enhancing the bandwidth by using wide-bandgap devices or advanced topologies will increase the total cost of the test bench, and control algorithms with high control bandwidth will burden the digital processor. Anti-aliasing filters can be implemented to reduce the sampling errors, but they are not suitable for the converter under test and the current ripples still exist. More effective methods are needed to meet these challenges.

References

[1] D. Ronanki, S. A. Singh, and S. S. Williamson, "Comprehensive topological overview of rolling stock architectures and recent trends in electric railway traction systems," *IEEE Trans. Transp. Electrific.*, vol. 3, no. 3, pp. 724–738, Sep. 2017.

[2] E. Bostanci, M. Moallem, A. Parsapour, and B. Fahimi, "Opportunities and challenges of switched reluctance motor drives for electric propulsion: A comparative study," *IEEE Trans. Transp. Electrific.*, vol. 3, no. 1, pp. 58–75, Mar. 2017.

[3] M. Morandin, A. Faggion, and S. Bolognani, "Integrated starter–alternator with sensorless ringed-pole PM synchronous motor drive," *IEEE Trans. Ind. Appl.*, vol. 51, no. 2, pp. 1485–1493, Mar./Apr. 2015.

[4] K.-W. Hu and C.-M. Liaw, "Incorporated operation control of DC microgrid and electric vehicle," *IEEE Trans. Ind. Electron.*, vol. 63, no. 1, pp. 202–215, Jan. 2016.

[5] F. Gao, X. Zheng, S. Bozhko, C. I. Hill, and G. Asher, "Modal analysis of a PMSG-based DC electrical power system in the more electric aircraft using eigenvalues sensitivity," *IEEE Trans. Transp. Electrific.*, vol. 1, no. 1, pp. 65–76, Jun. 2015.

[6] H. Chen, "Switched reluctance motors drive for the electrical traction in shearer," in *Proc. CES/IEEE 5th Int. Power Electron. Motion Control Conf.*, Aug. 2006, pp. 1–4.

[7] W. Li, G. Joos, and J. Belanger, "Real-time simulation of a wind turbine generator coupled with a battery supercapacitor energy storage system," *IEEE Trans. Ind. Electron.*, vol. 57, no. 4, pp. 1137–1145, Apr. 2010.

[8] H. Kubota and K. Matsuse, "Speed sensorless field-oriented control of induction motor with rotor resistance adaptation," *IEEE Trans. Ind. Appl.*, vol. 30, no. 5, pp. 1219–1224, Sep./Oct. 1994.

[9] J. Lara, J. Xu, and A. Chandra, "Effects of rotor position error in the performance of field-oriented-controlled PMSM drives for electric vehicle traction applications," *IEEE Trans. Ind. Electron.*, vol. 63, no. 8, pp. 4738–4751, Aug. 2016.

[10] S. S. Sebtahmadi, H. Pirasteh, S. H. Aghay Kaboli, A. Radan, and S. Mekhilef, "A 12-sector space vector switching scheme for performance improvement of matrix-converter-based DTC of IM drive," *IEEE Trans. Power Electron.*, vol. 30, no. 7, pp. 3804–3817, Jul. 2015.

[11] D. Mohan, X. Zhang, and G. H. B. Foo, "A simple duty cycle control strategy to reduce torque ripples and improve low-speed performance of a three-level inverter fed DTC IPMSM drive," *IEEE Trans. Ind. Electron.*, vol. 64, no. 4, pp. 2709–2721, Apr. 2017.

[12] S. Chen and S. N. Yeh, "Optimal efficiency analysis of induction motors fed by variable-voltage and variable-frequency source," *IEEE Trans. Energy Convers.*, vol. 7, no. 3, pp. 537–543, Sep. 1992.

[13] F. Blaabjerg and K. Ma, "Future on power electronics for wind turbine systems," *IEEE J. Emerg. Sel. Topics Power Electron.*, vol. 1, no. 3, pp. 139–152, Sep. 2013.

[14] F. Blaabjerg and K. Ma, "Wind energy systems," *Proc. IEEE*, vol. 105, no. 11, pp. 2116–2131, Nov. 2017.

[15] K. Ma, M. Liserre, F. Blaabjerg, and T. Kerekes, "Thermal loading and lifetime estimation for power device considering mission profiles in wind power converter," *IEEE Trans. Power Electron.*, vol. 30, no. 2, pp. 590–602, Feb. 2015.

[16] P. Sandholdt, E. Ritchie, J. K. Pedersen, and R. E. Betz, "A dynamometer performing dynamical emulation of loads with nonlinear friction," in *Proc. IEEE Int. Symp. Ind. Electron.*, 1996, vol. 2, pp. 873–878.

[17] Z. Hakan Akpolat, G. M. Asher, and J. C. Clare, "Dynamic emulation of mechanical loads using a vector-controlled induction motor-generator set," *IEEE Trans. Ind. Electron.*, vol. 46, no. 2, pp. 370–379, Apr. 1999.

[18] H. Azizi-Moghaddam, S. Mohamadian, and R. Nasiri-Zarandi, "Adaptive vector control of induction motor based inverse dynamic dynamometer," in *Proc. 11th Power Electron., Drive Syst., Technol. Conf.*, 2020, pp. 1–6.

[19] A. S. Vijay, S. Doolla, and M. C. Chandorkar, "Real-time testing approaches for microgrids," *IEEE J. Emerg. Sel. Topics Power Electron.*, vol. 5, no. 3, pp. 1356–1376, Sep. 2017.

[20] M. Steurer, C. S. Edrington, M. Sloderbeck, W. Ren, and J. Langston, "A megawatt-scale power hardware-in-the-loop simulation setup for motor drives," *IEEE Trans. Ind. Electron.*, vol. 57, no. 4, pp. 1254–1260, Apr. 2010.

[21] V. Karapanos, S. de Haan, and K. Zwetsloot, "Real time simulation of a power system with VSG hardware in the loop," in *Proc. IEEE Ind. Electron. Soc. Conf.*, Nov. 2011, pp. 3748–3754.

[22] P. Kotsampopoulos, A. Kapetanaki, G. Messinis, V. Kleftakis, and N. Hatziargyriou, "A PHIL facility for microgrids," *Int. J. Distrib. Energy Resour.*, vol. 9, no. 1, pp. 71–86, Mar. 2013.

[23] J. Wang, L. Yang, Y. Ma, L. M. Tolbert, F. Wang, and K. Tomsovic, "Static and dynamic power system load emulation in a converter-based reconfigurable power grid emulator," *IEEE Trans. Power Electron.*, vol. 31, no. 4, pp. 3239–3251, Apr. 2016.

[24] K. Ma, J. Wang, X. Cai, and F. Blaabjerg, "AC grid emulations for advanced testing of grid-connected converters—An overview," *IEEE Trans. Power Electron.*, vol. 36, no. 2, pp. 1626–1645, Feb. 2021.

[25] H. J. Slater, D. J. Atkinson, and A. G. Jack, "Real-time emulation for power equipment development—II. The virtual machine," *Proc. Inst. Elect. Eng., Elect. Power Appl.*, vol. 145, no. 3, pp. 153–158, May 1998.

[26] A. M. Dudley, "Notes on methods of making load tests on large induction motors," *Proc. Amer. Inst. Elect. Eng.*, vol. 32, no. 2, pp. 617–626, Feb. 1913.

[27] M. F. Sedlar, "IRDIS: An image processing system for hardware-in-the-loop missile testing," in *Proc. IEEE Nat. Aerosp. Electron. Conf.*, May 1989, vol. 2, pp. 869–874.

[28] I. Vernica, F. Blaabjerg, and K. Ma, "Mission profile emulator for the power electronics systems of motor drive applications," in *Proc. 19th Eur. Conf. Power Electron. Appl.*, 2017, pp. P.1–P.10.

[29] S. Chakraborty *et al.*, "Real-life mission profile oriented lifetime estimation of a SiC interleaved bidirectional HV DC/DC converter for electric vehicle drivetrains," *IEEE J. Emerg. Sel. Topics Power Electron.*, to be published, doi: 10.1109/JESTPE.2021.3083198.

[30] S. Singhal, H. Walter, and T. Tyer, "Concept, design and testing of a 12 MW 9500 RPM induction motor with oil film bearings for pipeline applications in North America," in *Proc. IEEE IAS Annu. Petroleum Chem. Ind. Conf.*, Sep. 2013, pp. 1–16.

[31] S. Singhal, "Electric drive compressor systems: High-speed turbo compressors used in the oil and gas industry," *IEEE Ind. Appl. Mag.*, vol. 20, no. 6, pp. 52–63, Nov./Dec. 2014.

[32] W. R. Finley, M. M. Hodowanec, and W. G. Holter, "An analytical approach to solving motor vibration problems," *IEEE Trans. Ind. Appl.*, vol. 36, no. 5, pp. 1467–1480, Sep./Oct. 2000.

[33] K. Saito and H. Akagi, "A real-time real-power emulator for a medium-voltage high-speed electrical drive: Discussion on mechanical vibrations," *IEEE Trans. Ind. Appl.*, vol. 57, no. 2, pp. 1482–1494, Mar./Apr. 2021.

[34] Y. Tan, J. Chang, and H. Tan, "Adaptive backstepping control and friction compensation for AC servo with inertia and load uncertainties," *IEEE Trans. Ind. Electron.*, vol. 50, no. 5, pp. 944–952, Oct. 2003.

[35] Y. Guan, Y. Wu, Y. Gao, and X. Liu, "Multi-motor synchronous servo system control based on improved inertia identification," in *Proc. 5th Int. Conf. Inf., Cybern., Comput. Social Syst.*, 2018, pp. 270–274.

[36] S. Li and Z. Liu, "Adaptive speed control for permanent-magnet synchronous motor system with variations of load inertia," *IEEE Trans. Ind. Electron.*, vol. 56, no. 8, pp. 3050–3059, Aug. 2009.

[37] J. Jung and K. Nam, "A dynamic decoupling control scheme for high-speed operation of induction motors," *IEEE Trans. Ind. Electron.*, vol. 46, no. 1, pp. 100–110, Feb. 1999.

[38] J. Lu, J. Yang, Y. Ma, and R. Ren, "Compensation for harmonic flux and current of permanent magnet synchronous motor by harmonic voltage," in *Proc. Int. Conf. Informat., Electron. Vis.*, 2015, pp. 1–5.

[39] T. Nakai and H. Fujimoto, "Harmonic current suppression method of PMSM based on repetitive perfect tracking control," in *Proc. 33rd Annu. Conf. IEEE Ind. Electron. Soc.*, Nov. 2007, pp. 1049–1054.

[40] K. S. Amitkumar, P. Pillay, and J. Bélanger, "An investigation of power-hardware-in-the-loop- based electric machine emulation for driving inverter open-circuit faults," *IEEE Trans. Transp. Electrific.*, vol. 7, no. 1, pp. 170–182, Mar. 2021.

[41] F. Alvarez-Gonzalez, A. Griffo, B. Sen, and J. Wang, "Real-time hardware-in-the-loop simulation of permanent-magnet synchronous motor drives under stator faults," *IEEE Trans. Ind. Electron.*, vol. 64, no. 9, pp. 6960–6969, Sep. 2017.

[42] S. Nandi, H. A. Toliyat, and X. Li, "Condition monitoring and fault diagnosis of electrical motors—A review," *IEEE Trans. Energy Convers.*, vol. 20, no. 4, pp. 719–729, Dec. 2005.

[43] E. Agamloh, S. Vaschetto, A. Cavagnino, A. von Jouanne, and A. Yokochi, "Alternative methods for electric machine rated load temperature tests," in *Proc. IEEE Energy Convers. Congr. Expo.*, Oct. 2020, pp. 2081–2088.

[44] F. Ghoroghchian, A. D. Aliabad, and E. Amiri, "Dual-pole LSPM motor with dahlander winding for high inertia loads," in *Proc. IEEE 28th Int. Symp. Ind. Electron.*, Jun. 2019, pp. 308–312.

[45] C. Mao *et al.*, "A 400-V/50-kVA digital–physical hybrid real-time simulation platform for power systems," *IEEE Trans. Ind. Electron.*, vol. 65, no. 5, pp. 3666–3676, May 2018.

[46] A. Myaing and V. Dinavahi, "FPGA-based real-time emulation of power electronic systems with detailed representation of device characteristics," *IEEE Trans. Ind. Electron.*, vol. 58, no. 1, pp. 358–368, Jan. 2011.

[47] G. F. Lauss, M. O. Faruque, K. Schoder, C. Dufour, A. Viehweider, and J. Langston, "Characteristics and design of power hardware-in-the-loop simulations for electrical power systems," *IEEE Trans. Ind. Electron.*, vol. 63, no. 1, pp. 406–417, Jan. 2016.

[48] M. K. Namboothiripad, M. J. Datar, M. C. Chandorkar, and S. B. Patkar, "FPGA accelerator for real-time emulation of power electronic systems using multiport decomposition," *IEEE Trans. Ind. Appl.*, vol. 56, no. 6, pp. 6674–6686, Nov./Dec. 2020.

[49] K. Upamanyu and G. Narayanan, "Improved accuracy, modeling, and stability analysis of power-hardware-in-loop simulation with open-loop inverter as power amplifier," *IEEE Trans. Ind. Electron.*, vol. 67, no. 1, pp. 369–378, Jan. 2020.

[50] M. Pokhare and C. N. M. Ho, "Stability analysis of power hardware-in-the-loop architecture with solar inverter," *IEEE Trans. Ind. Electron.*, vol. 68, no. 5, pp. 4309–4319, May 2021.

[51] S. Zhang, B. Liu, S. Zheng, Y. Ma, F. Wang, and L. M. Tolbert, "Development of a converter-based transmission line emulator with three-phase short-circuit fault emulation capability," *IEEE Trans. Power Electron.*, vol. 33, no. 12, pp. 10215–10228, Dec. 2018.

[52] B. D. Kelper, H. F. Blanchette, and L. A. Dessaint, "Switching time model updating for the real-time simulation of power-electronic circuits and motor drives," *IEEE Trans. Energy Convers.*, vol. 20, no. 1, pp. 181–186, Mar. 2005.

[53] C. Choi and W. Lee, "Analysis and compensation of time delay effects in hardware-in-the-loop simulation for automotive PMSM drive system," *IEEE Trans. Ind. Electron.*, vol. 59, no. 9, pp. 3403–3410, Sep. 2012.

[54] E. Guillo-Sansano, M. H. Syed, A. J. Roscoe, G. M. Burt, and F. Coffele, "Characterization of time delay in power hardware in the loop setups," *IEEE Trans. Ind. Electron.*, vol. 68, no. 3, pp. 2703–2713, Mar. 2021.

[55] D. Pérez-Estévez, J. Doval-Gandoy, A. G. Yepes, Ó. López, and F. Baneira, "Enhanced resonant current controller for grid-connected converters with LCL filter," *IEEE Trans. Power Electron.*, vol. 33, no. 5, pp. 3765–3778, May 2018.

[56] Y. Qi, K. Ma, and W. Tang, "Full-bandwidth mission profile emulation of electric machine system with voltage reference signal transmission," *IEEE Trans. Power Electron.*, vol. 37, no. 3, pp. 3473–3483, Mar. 2022.

[57] X. Wang and F. Blaabjerg, "Harmonic stability in power electronic-based power systems: Concept, modeling, and analysis," *IEEE Trans. Smart Grid*, vol. 10, no. 3, pp. 2858–2870, May 2019.

[58] K. Ma, W. Tang, R. Cheng, and Y. Song, "Modeling of interconnected voltage and current controlled converters with coupled LC–LCL filters," *IEEE Trans. Power Electron.*, vol. 36, no. 4, pp. 3995–4005, Apr. 2021.

[59] K. Saito and H. Akagi, "A real-time real-power emulator of a medium-voltage high-speed induction motor loaded with a centrifugal compressor," *IEEE Trans. Ind. Appl.*, vol. 55, no. 5, pp. 4821–4833, Sep./Oct. 2019.

[60] M. Steurer, C. S. Edrington, M. Sloderbeck, W. Ren, and J. Langston, "A megawatt-scale power hardware-in-the-loop simulation setup for motor drives," *IEEE Trans. Ind. Electron.*, vol. 57, no. 4, pp. 1254–1260, Apr. 2010.

[61] G. Gong, D. Hassler, and J. W. Kolar, "A comparative study of multicell amplifiers for AC-power-source applications," *IEEE Trans. Power Electron.*, vol. 26, no. 1, pp. 149–164, Jan. 2011.

[62] Y. Lee, Y. Kwon, and S. Sul, "DC-link voltage design of high-bandwidth motor emulator for interior permanent-magnet synchronous motors," in *Proc. IEEE Energy Convers. Congr. Expo.*, Sep. 2018, pp. 4453–4459.

[63] P. C. Krause, O. Wasynczuk, and S. D. Sudhoff, *Analysis of Electric Machinery and Drive Systems*. Hoboken, NJ, USA: Wiley, 2002, pp. 191–206.

[64] C. Capitan, *Torque Control in Field Weakening Mode*. Aalborg, Denmark: Aalborg Univ. Press, 2009, pp. 7–14.

[65] I. Vernica, *Modelling and Implementation of Active Thermal Control Methods for Power Electronics Systems for Motor Drive Applications*. Aalborg, Denmark: Aalborg Univ. Press, 2016, pp. 7–16.

[66] N. R. Tavana and V. Dinavahi, "Real-time FPGA-based analytical space harmonic model of permanent magnet machines for hardware-in-the-loop simulation," *IEEE Trans. Magn.*, vol. 51, no. 8, Aug. 2015, Art. no. 8106609.

[67] M. A. Masadeh, K. S. Amitkumar, and P. Pillay, "Power electronic converter-based induction motor emulator including main and leakage flux saturation," *IEEE Trans. Transp. Electrific.*, vol. 4, no. 2, pp. 483–493, Jun. 2018.

[68] K. S. Amitkumar, R. Thike, and P. Pillay, "Linear amplifier-based power-hardware-in-the-loop emulation of a variable flux machine," *IEEE Trans. Ind. Appl.*, vol. 55, no. 5, pp. 4624–4632, Sep./Oct. 2019.

[69] Y. Song, R. Cheng, and K. Ma, "Mission profile emulator for permanent magnet synchronous machine in voltage-response mode based on three-phase power electronic converter," in *Proc. IEEE Int. Power Electron. Appl. Conf. Expo.*, Nov. 2018, pp. 1–5.

[70] K. Ma and Y. Song, "Power-electronic-based electric machine emulator using direct impedance regulation," *IEEE Trans. Power Electron.*, vol. 35, no. 10, pp. 10673–10680, Oct. 2020.

[71] K. S. Amitkumar, R. S. Kaarthik, and P. Pillay, "A versatile power-hardware-in-the-loop-based emulator for rapid testing of transportation electric drives," *IEEE Trans. Transp. Electrific.*, vol. 4, no. 4, pp. 901–911, Dec. 2018.

[72] G. Tanuku and P. Pillay, "Induction machine emulation under asymmetric grid faults," in *Proc. IEEE Energy Convers. Congr. Expo.*, Oct. 2020, pp. 2351–2356.

[73] Y. Song, R. Cheng, and K. Ma, "Harmonics suppression and control design for general-purpose mission profile emulator of three-phase power electronics system," in *Proc. IEEE Energy Convers. Congr. Expo.*, Sep. 2018, pp. 5713–5718.

[74] R. Bojoi, E. Armando, S. G. Rosu, S. Vaschetto, and P. Soccio, "Virtual load with common mode active filtering for power hardware-in-the-loop testing of power electronic converters," in *Proc. Annu. Conf. IEEE Ind. Electron. Soc.*, 2014, pp. 1875–1881.

[75] O. Vodyakho, M. Steurer, C. S. Edrington, and F. Fleming, "An induction machine emulator for high-power applications utilizing advanced simulation tools with graphical user interfaces," *IEEE Trans. Energy Convers.*, vol. 27, no. 1, pp. 160–172, Mar. 2012.

[76] Y. Luo, M. A. Awal, W. Yu, and I. Husain, "FPGA based high bandwidth motor emulator for interior permanent magnet machine utilizing SiC power converter," *IEEE J. Emerg. Sel. Topics Power Electron.*, vol. 9, no. 4, pp. 4340–4353, Aug. 2021.

[77] Y. Srinivasa Rao and M. C. Chandorkar, "Real-time electrical load emulator using optimal feedback control technique," *IEEE Trans. Ind. Electron.*, vol. 57, no. 4, pp. 1217–1225, Apr. 2010.

[78] S. Grubic, B. Amlang, W. Schumacher, and A. Wenzel, "A high-performance electronic hardware-in-the-loop drive–load simulation using a linear inverter (LinVerter)," *IEEE Trans. Ind. Electron.*, vol. 57, no. 4, pp. 1208–1216, Apr. 2010.

[79] G. Si, J. Cordier, and R. M. Kennel, "Extending the power capability with dynamic performance of a power-hardware-in-the-loop application—Power grid emulator using 'inverter cumulation'," *IEEE Trans. Ind. Appl.*, vol. 52, no. 4, pp. 3193–3202, Jul./Aug. 2016.

[80] T. Roinila *et al.*, "Hardware-in-the-loop methods for real-time frequency response measurements of on-board power distribution systems," *IEEE Trans. Ind. Electron.*, vol. 66, no. 7, pp. 5769–5777, Jul. 2019.

[81] S. Lentijo, S. D'Arco, and A. Monti, "Comparing the dynamic performances of power hardware-in-the-loop interfaces," *IEEE Trans. Ind. Electron.*, vol. 57, no. 4, pp. 1195–1207, Apr. 2010.

[82] J. Shen *et al.*, "A high-frequency high-power test bench for 11 MW/595 Hz drives with 1.25MWgrid capability," *IEEE Trans. Ind. Appl.*, vol. 53, no. 5, pp. 4744–4756, Sep./Oct. 2017.

[83] M. H. Bierhoff and F. W. Fuchs, "DC-link harmonics of three-phase voltage-source converters influenced by the pulsewidth-modulation strategy—An analysis," *IEEE Trans. Ind. Electron.*, vol. 55, no. 5, pp. 2085–2092, May 2008.

[84] D. Zhang, F. Wang, R. Burgos, R. Lai, and D. Boroyevich, "DC-link ripple current reduction for paralleled three-phase voltage-source converters with interleaving," *IEEE Trans. Power Electron.*, vol. 26, no. 6, pp. 1741–1753, Jun. 2011.

Ke Ma (Senior Member, IEEE) received the B.Sc. and M.Sc. degrees in electrical engineering from Zhejiang University, Hangzhou, China, in 2007 and 2010, respectively, and the Ph.D. degree from Aalborg University, Aalborg, Denmark, in 2013.

He became an Assistant Professor with Aalborg University in 2014. In 2016, he joined the faculty of Shanghai Jiao Tong University, China, as a tenure-track Research Professor, and is currently serving as the Deputy Director for the Key Laboratory of Control of Power Transmission and Conversion, Ministry of Education, China. His current research interests include the power electronics and its reliability in the application of renewable energy, HVdc, and motor drive systems.

Dr. Ma was the recipient of "Excellent Young Wind Doctor Award 2014" by European Academy of Wind Energy, and several prized paper awards by IEEE. He is currently serving as an Associate Editor for two IEEE Transaction journals, and the Vice Chair for two IEEE Technical Committees.

Shihao Xia received the B.Sc. degree in electrical engineering from Xi'an Jiaotong University, Xi'an, China, in 2020. He is currently working toward the Ph.D. degree with Shanghai Jiao Tong University, Shanghai, China.

His research interests include the stability and reliability of motor drive systems and mission profile emulation for motor drive systems.

Yuhao Qi (Graduate Student Member, IEEE) received the B.Sc. degree in electrical engineering in 2020 from Shanghai Jiao Tong University, Shanghai, China, where he is currently working toward the M.Sc. degree in electrical engineering.

His research interests include the modeling, analysis, and control of motor drive systems, and mission profile emulation for motor drive systems.

Xu Cai (Senior Member, IEEE) received the B.Eng. degree from Southeast University, Nanjing, China, in 1983, the M.Eng. and Ph.D. degrees from the China University of Mining and Technology, Jiangsu, China, in 1988 and 2000, respectively, all in electrical engineering.

Since 2002, he was a Professor with the Department of Electrical Engineering, China University of Mining and Technology, as an Associate Professor, from 1989 to 2001. He was the Vice Director of the State Energy Smart Grid R&D Center, Shanghai, China, from 2010 to 2013. Since 2002, he has been a Professor with Shanghai Jiao Tong University, Shanghai, where he has also been the Director of the Wind Power Research Center since 2008. His current research interests include power electronics and renewable energy exploitation and utilization, including wind power converters, wind turbine control system, large power battery storage systems, clustering of wind farms and its control system, and grid integration.

Yubo Song (Senior Member, IEEE) received the B.Sc. and M.Sc. degrees in electrical engineering from Shanghai Jiao Tong University, Shanghai, China, in 2016 and 2019, respectively. He is currently working toward the Ph.D. degree with Aalborg University, Aalborg, Denmark.

His research interests include the stability and reliability of microgrid systems, and mission profile emulation for motor drive systems.

Frede Blaabjerg (Fellow, IEEE) received the honoris causa degree from the University Politehnica Timisoara, Timisoara, Romania, in 2017, and Tallinn Technical University, Tallinn, Estonia, in 2018, and the Ph.D. degree in electrical engineering from Aalborg University, Aalborg, Denmark, in 1995.

He was with ABB-Scandia, Randers, Denmark, from 1987 to 1988. He was an Assistant Professor with Aalborg University, in 1992, an Associate Professor, in 1996, and a Full Professor of power electronics and drives, in 1998. Since 2017, he has been a Villum Investigator. He has authored or coauthored more than 600 journal papers in the fields of power electronics and its applications. He has coauthored four monographs and editor of ten books in power electronics and its applications. His current research interests include power electronics and its applications such as in wind turbines, PV systems, reliability, harmonics, and adjustable speed drives.

Dr. Blaabjerg was the recipient of 33 IEEE Prize Paper Awards, the IEEE PELS Distinguished Service Award in 2009, the EPE-PEMC Council Award in 2010, the IEEE William E. Newell Power Electronics Award 2014, the Villum Kann Rasmussen Research Award 2014, the Global Energy Prize in 2019 and the 2020 IEEE Edison Medal. He was the Editor-in-Chief for the IEEE TRANSACTIONS ON POWER ELECTRONICS from 2006 to 2012. He has been a Distinguished Lecturer for the IEEE Power Electronics Society from 2005 to 2007 and for the IEEE Industry Applications Society from 2010 to 2011 as well as 2017 to 2018. In 2019 and 2020, he was the President of IEEE Power Electronics Society. He has been the Vice-President of the Danish Academy of Technical Sciences. He is nominated in 2014–2020 by Thomson Reuters to be between the most 250 cited researchers in Engineering in the world.